Role of metabolic pathways and sensors in regulation of dendritic cell-driven T cell responses

Pelgrom, L.R.

4

Cell-Intrinsic Glycogen Metabolism Supports Early Glycolytic Reprogramming Required for Dendritic Cell Immune Responses

Phyu M. Thwe
Leonard R. Pelgrom
Rachel Cooper
Saritha Beauchamp
Julie A. Reisz
Angelo D'Alessandro
Bart Everts
Eyal Amiel

Cell Metab. 2019 Jul 2;30(1):225
PMID: 31269426
DOI: 10.1016/j.cmet.2019.05.017

Summary

Dendritic cell (DC) activation by Toll-like receptor (TLR) agonists causes rapid glycolytic reprogramming that is required to meet the metabolic demands of their immune activation. Recent efforts in the field have identified an important role for extracellular glucose sourcing to support DC activation. However, the contributions of intracellular glucose stores to these processes have not been well characterized. We demonstrate that DCs possess intracellular glycogen stores and that cell-intrinsic glycogen metabolism supports the early effector functions of TLR-activated DCs. Inhibition of glycogenolysis significantly attenuates TLR-mediated DC maturation and impairs their ability to initiate lymphocyte activation. We further report that DCs exhibit functional compartmentalization of glucose- and glycogen-derived carbons, where these substrates preferentially contribute to distinct metabolic pathways. This work provides novel insights into nutrient homeostasis in DCs, demonstrating that differential utilization of glycogen and glucose metabolism regulates their optimal immune function.

Introduction

Dendritic cells (DCs) are canonical ''professional antigen presenting cells'' of the immune system and play a central role in coordinating both innate and adaptive immune responses [1-3]. DCs recognize microbial pathogens and other inflammatory stimuli through the expression of innate immune receptors including the Toll-like receptor (TLR) family [4-6]. DC activation by TLR signaling initiates a complex set of transcriptional and translational events that are characterized by the upregulation of surface co-stimulatory molecule expression, inflammatory cytokine secretion, and the ability to stimulate T lymphocytes via antigen presentation by major histocompatibility (MHC) molecules.

TLR stimulation initiates a shift in DC metabolism characterized by upregulation of aerobic glycolysis, which plays a vital role in supporting the immune effector function and survival of both human and mouse DCs [7-10]. Rapid glycolysis induction supports the metabolic requirements associated with the high levels of protein synthesis that contribute to DC immune activity. The TLR-mediated ''glycolytic burst'' drives *de novo* fatty acid synthesis via glucose-dependent citrate metabolism, which supports the synthesis and secretion of inflammatory cytokines [8, 11]. Interrupting the glucose-to-citrate pathway significantly impairs DC maturation, cytokine secretion, and T cell stimulatory capacity [8-10].

Immune cells are thought to primarily support activation-associated glycolysis via increased expression of glucose transporters [12-15]. Consistent with this, the role of the inducible glucose transporter, GLUT1, in regulating activation-associated glucose flux in both myeloid and lymphoid immune cells has been a major focus in the field [16, 17]. In DCs, however, GLUT1 upregulation occurs several hours after TLR stimulation, while TLR-mediated glycolytic reprogramming happens within minutes of activation. Thus, the source of glucose supporting the earliest events in DC activation, namely whether glucose is sourced from the extracellular environment or from intracellular pools, has not been fully defined. We propose that the DCs utilize intracellular glycogen reserves to fuel their metabolic needs during early immune activation and that glycogen metabolism is required by these cells to initiate proper immune effector responses.

Glycogen, a large branch-chained glucose polymer, has been extensively characterized in hepatocytes, muscle cells, and neuronal tissue where it serves as an intracellular carbon reservoir [18-20]. Cells in the liver, muscle, and brain express tissue-specific enzymes for glycogen synthase (GYS) and glycogen phosphorylase (PYG), the rate-limiting enzymes of glycogen synthesis and breakdown, respectively. Cells in these tissues store glucose in the form of

glycogen to be utilized according to their specific metabolic demands [18-20]. During glycogenolysis, PYG isozymes break down glycogen into glucose-1-phosphate (G1P), which is subsequently converted into glucose-6-phosphate (G6P) and can serve as a direct substrate for further catabolism via glycolysis. In this manner, glycogen-storing cells, such as those in muscle and brain tissue, can maintain intracellular glycogen reserves for cell-intrinsic metabolic requirements [18, 20]. The significance of cell-intrinsic glycogen metabolism in immune cells has not been well characterized.

We demonstrate that DCs express specific isoforms of enzymes essential for glycogen synthesis and breakdown and that these cells require glycogen metabolism to support their immune function. Although the presence of glycogen in DCs has been previously implicated [21], the direct role for glycogen in DC metabolism and immune function has not been described. We propose that DCs use intracellular glycogen reserves to support early glycolytic metabolism that accompanies their activation. We show that disruption of glycogen metabolism significantly impairs DC maturation and immune effector function, particularly at early stages of activation and in glucose-restricted conditions. We further show that glycogen-derived carbons preferentially contribute to the TCA- dependent citrate pool compared to glucose catabolized directly by the cell. These findings elucidate a novel metabolic regulatory pathway in DCs and provide new insights into energy and nutrient homeostasis in these cells in support of their immune activation.

Results and discussion

DCs Express Glycogen Metabolic Machinery and Utilize Cell-Intrinsic Glycogen Metabolism upon Activation

TLR stimulation drives DCs to undergo glycolytic reprogramming in order to meet cellular anabolic demands associated with activation [8, 10]. We performed a nutrient screening assay using single-carbon-source defined media and found that DCs can catabolize both short- and long-chain glucose polymers (Figure 1A). The ability of DCs to generate NADH from glycogen (Figure 1A) is of particular interest given its role as the predominant form of glucose macromolecule storage in normal physiology. While cells are unlikely to encounter extracellular glycogen *in vivo*, these assays demonstrate that DCs exhibit the capability to catabolize glycogen and are likely to express the key enzymes of glycogen metabolism.

We analyzed mRNA levels of glycogen phosphorylase (PYG) and glycogen synthase (GYS), the rate-limiting enzymes of glycogen breakdown and synthesis pathways, respectively in DCs. Glycogenolysis is executed by three

different tissue-specific PYG isozymes in mice and humans: PYGL in the liver, PYGM in muscle, and PYGB in brain tissue. Glycogen synthesis is controlled by two different tissue-specific GYS isozymes: GYS1 in muscles and other peripheral tissue, and GYS2 in the liver. Both mRNA and protein analysis in mouse bone marrow-derived DCs (BMDCs) (Figures 1B and 1C) and human monocyte-derived DCs (moDCs) (Figure 1D) showed that DCs express PYGL and GYS1 isozymes. These enzymes were not appreciably regulated following 6 hr stimulation with LPS (Figures 1C and 1D). Detection of intracellular glycogen in freshly isolated human $CD14^+$ monocytes and $CD1a^+$ dendritic cells (Figure 1E) indicates a physiological role for glycogen in these cells. Unactivated DCs contain intracellular glycogen pools that are fully depleted when cells are cultured in glucose-free media (Figure 1F) and partially depleted by LPS stimulation in BMDCs (Figure 1G) and moDCs (Figure 1H). TEM images of BMDCs show distinct glycogen deposits by tannic acid stain that are absent in cells grown without glucose (Figure 1I) [22].

To validate the efficacy and specificity of the PYG inhibitor, CP91149 (CP), we incubated BMDCs with CP in the nutrient screening assay (as in Figure 1A) and assessed inhibition of glucose or glycogen catabolism. Glycogen-dependent NADH levels were fully attenuated in the presence of CP, while glucose-dependent NADH levels were unaffected (Figure 1J), demonstrating the specificity of this inhibitor. PYG inhibition caused a reduction in basal glycolysis rates in unactivated BMDCs (Figure 1K), indicating that DCs utilize intracellular glycogen to support basal glycolytic demands. Importantly, the effect of glycolysis inhibitor 2-deoxyglucose (2DG) was non-redundant with CP, showing that free glucose and intracellular glycogen stores make distinct contributions to DC metabolism (Figure 1K).

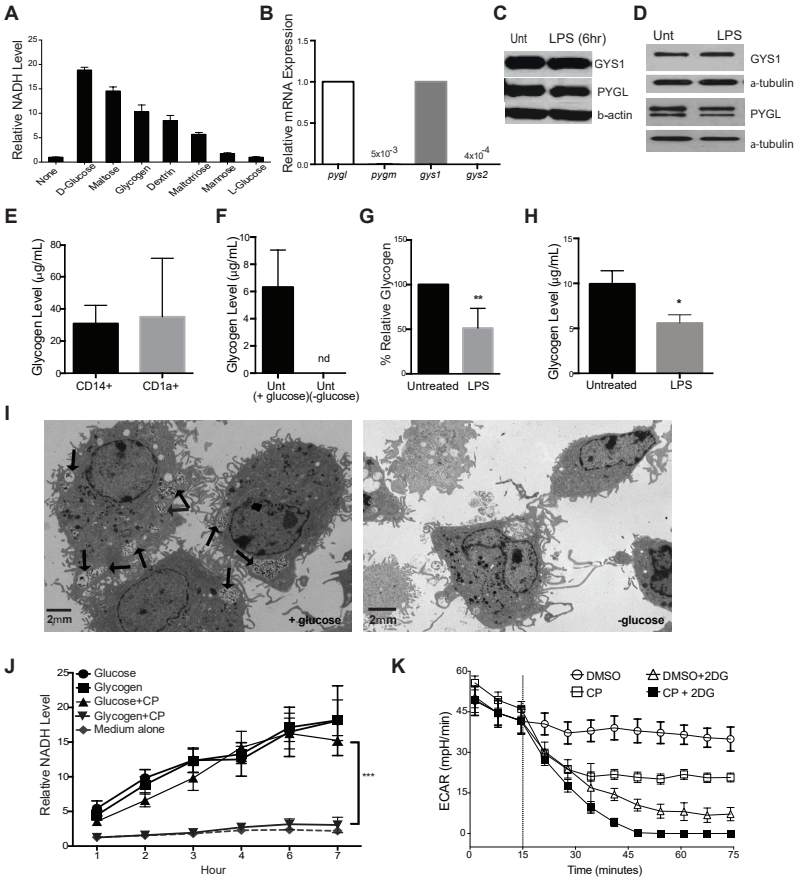
A
Relative NADH Level
None
D-Glucose
Maltose
Glycogen
Dextrin
Maltotriose
Mannose
L-Glucose
B
Relative mRNA Expression
pygl
pygm
gys1
gys2
C
Unt
LPS (6hr)
GYS1
PYGL
b-actin
D
Unt
LPS
GYS1
a-tubulin
PYGL
a-tubulin
E
Glycogen Level (μg/mL)
CD14+
CD1a+
F
Glycogen Level (μg/mL)
nd
Unt (+ glucose)
Unt (-glucose)
G
% Relative Glycogen
Untreated
LPS
H
Glycogen Level (μg/mL)
Untreated
LPS
I
2mm
+ glucose
2mm
-glucose
J
Glucose
Glycogen
Glucose+CP
Glycogen+CP
Medium alone
Relative NADH Level
Hour
K
DMSO
DMSO+2DG
CP
CP + 2DG
ECAR (mpH/min)
Time (minutes)

Figure 1. DCs Utilize Intracellular Glycogen Metabolism upon LPS Stimulation.

(A) BMDCs were cultured in the indicated substrates as the sole nutrient sources and measured for ability to produce NADH as described in STAR Methods. Data indicate relative NADH production at 6 hr normalized to no carbon source controls, n = 3.
(B) Relative mRNA expression of PYG and GYS isoforms in naive BMDCs.
(C and D) PYGL, GYS1, and β-actin protein expression in unactivated and 6 hr LPS-stimulated BMDCs (C) and 24 hr LPS-stimulated moDCs (D).
(E–H) Intracellular glycogen levels of human peripheral blood $CD14^+$ monocytes and $CD1a^+$ DCs (E), untreated BMDCs cultured overnight ± glucose (F), and BMDCs (G) and moDCs (H) stimulated ± LPS in 5 mM glucose (n = 3–6, mean ± SD, Student's t test, *p < 0.05, **p = 0.0021, nd = not detected). Glycogen levels were normalized to 10^5 cells.
(I) TEM images of unactivated BMDCs in 5 mM glucose (left) and 0 mM glucose (right), with arrows indicating intracellular glycogen deposits identified by tannic acid staining.
(J) NADH levels over time in BMDCs cultured in glucose or glycogen containing media (as in A) ± CP (n = 4, mean ± SD, ***p < 0.0001).
(K) Basal ECAR of resting BMDCs treated with CP, 2DG, or both (treatment introduced at dotted line); representative of at least three replicates.

PYG Inhibition Impacts DC Survival in Hypoglycemic Conditions

Glycogen metabolism supports cancer cell growth, proliferation, and cellular lifespan [23]. We tested the effect of PYG inhibition on the survival of BMDCs at early (6 hr) and late (24 hr) time points after LPS activation. PYG inhibition resulted in modest increases in cell death at early time points under low-glucose conditions (Figure 2A). This phenotype was increased after 24 hr of inhibition (Figure 2B). In contrast, the viability of human moDCs was not impacted at all glucose concentrations tested (Figure 2C).

Glycogen Metabolism Preferentially Supports Early DC Maturation

TLR-driven early glycolytic burst is a metabolic hallmark of activated DCs [24], and both lymphoid and myeloid cells depend heavily on extracellular glucose for glycolysis-dependent effector responses [9, 10, 15, 25]. This may pose a limitation on the abundance of glucose in highly inflamed tissues and secondary lymphoid organs where DCs likely experience nutrient competition with proliferating lymphocytes [26]. We hypothesized that glycogen metabolism supports early TLR-mediated glycolysis and activation in DCs by providing an intracellular source of glucose carbons. We examined the surface expression of CD40 and CD86 in BMDCs stimulated with LPS for 6 and 24 hr in the presence or absence of PYG inhibitor over a range of glucose concentrations representing both hyper- and hypoglycemic states. CD40 and CD86 expression was attenuated by CP treatment (Figures 2D and S1A), with a more pronounced effect at 6 hr and in hypoglycemic conditions (Figures 2D and S1A). PYG inhibition with an alternative inhibitor, DAB, at 6 hr after stimulation gave similar outcomes (Figure S1B). Reduced CD40 and CD86 expression was observed both in BMDCs starved of intracellular sugar (Figure 2E) and in moDCs inhibited

by CP (Figure 2F), further suggesting a role for glycogen pools in sustaining DC maturation. In addition, PYG-targeted siRNA was used to silence PYG expression in moDCs. As mRNA expression data indicated that both PYGB and PYGL isoenzymes are expressed in human moDCs (Figure S1C), both isoforms were silenced simultaneously in moDCs using targeted siRNA (Figure S1D). Genetic silencing of PYG in moDCs resulted in attenuation of LPS- induced expression of maturation markers (Figure 2G).

While the importance of GLUT1 has been conclusively delineated in both myeloid and lymphoid immune cells [8, 16, 17, 27], the kinetics of GLUT1 regulation do not account for the acute glycolytic reprogramming that occurs in activated DCs. GLUT1 upregulation in activated DCs is not detected before 6 hr of LPS stimulation (Figure S1E), which correlates with the finding that extracellular glucose is depleted only after 6 hr of stimulation (Figure 2H). To confirm that the cells are less dependent on imported glucose for early activation, we assessed DC maturation at 6 and 24 hr after LPS stimulation while blocking GLUT1 activity with inhibitor STF31 (Figures 2I and S1F). In contrast to PYG inhibition, GLUT1 inhibition had a significant impact on the maturation at 24 hr but not 6hrs after activation. These data provide strong evidence that cell-intrinsic glycogen metabolism plays a central role in driving DC maturation, particularly during early time points and in glucose-restricting conditions.

PYG Inhibition Impacts DC Immune Effector Function

Blocking glycolysis in TLR-activated DCs impairs their ability to produce inflammatory cytokines and stimulate T cells [8, 10]. We tested whether these responses are also affected by PYG inhibition. Intracellular cytokine staining for TNF-α and IL-12 after 4 hr of LPS stimulation showed that PYG inhibition attenuates inflammatory cytokine production, with a larger effect in low-glucose conditions (Figures 3A, 3B, and S2A). Multiplex cytokine analysis of LPS-stimulated DCs showed reduced pro-inflammatory cytokines and chemokine production in PYG-inhibited cells compared to controls in both BMDCs (Figure 3C) and moDCs (Figure 3D). CP did not globally impact all LPS-mediated protein production as other cytokines were unaffected (Figures S2B and S2C). siRNA-mediated knockdown of PYG expression in moDCs recapitulated the inhibitor data, as LPS-driven IL-12 production was attenuated in PYG-silenced moDCs (Figure 3E).

To examine the ability of DCs to take up and process antigens, we stimulated BMDCs with LPS plus OVA-AF488 or OVA-DQ for 3 hr (Figure 3F). OVA-AF488 allows tracking of antigen uptake, while OVA-DQ only fluoresces upon antigen uptake and processing. PYG-inhibited DCs showed reduced antigen uptake regardless of LPS stimulation (Figure 3F), while antigen processing was

unexpectedly enhanced by PYG inhibition. We next tested the effect of PYG inhibition or silencing on DC ability to stimulate $CD4^+$ T cells. PYG-inhibited BMDCs exhibited significantly reduced capacity to stimulate T cells (Figures 3G and 3H). PYG-silenced moDCs exhibited similar impairments in $CD4^+$ T cell stimulation (Figure 3I). These data demonstrate that cell-intrinsic glycogen metabolism contributes to the regulation of the multifaceted dimensions of DC immune effector function.

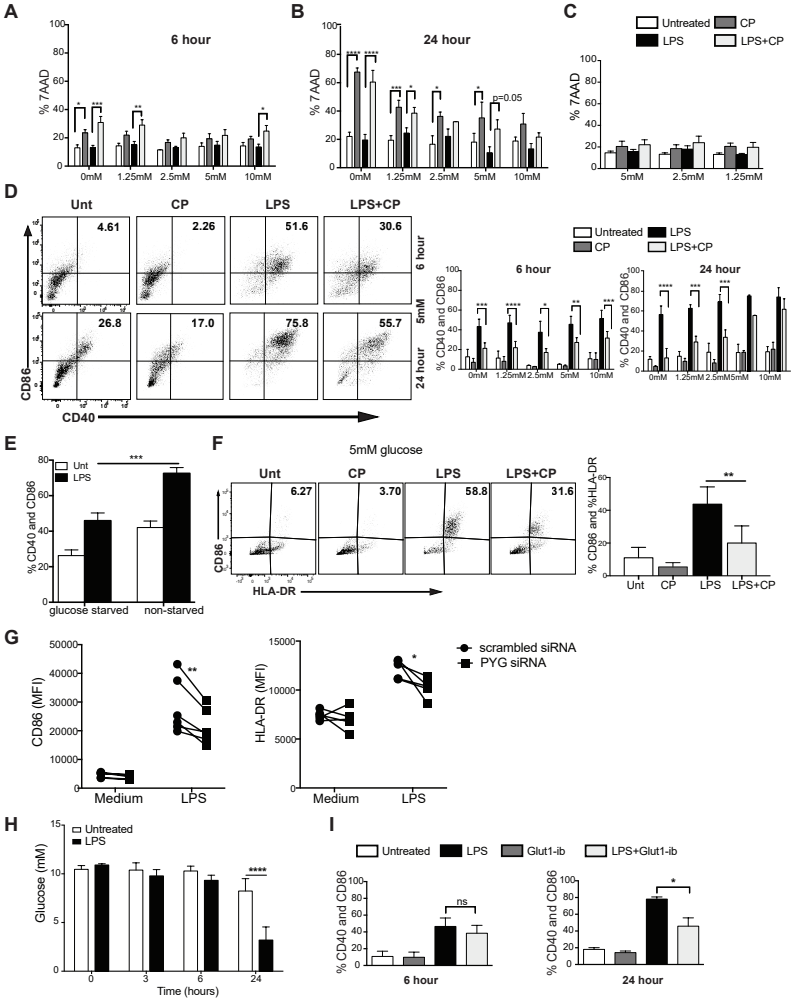
A
6 hour
% 7AAD
0mM 1.25mM 2.5mM 5mM 10mM
B
24 hour
% 7AAD
p=0.05
C
Untreated
CP
LPS
LPS+CP
% 7AAD
5mM 2.5mM 1.25mM
D
Unt
CP
LPS
LPS+CP
4.61
2.26
51.6
30.6
26.8
17.0
75.8
55.7
6 hour
5mM
24 hour
CD86
CD40
% CD40 and CD86
E
Unt
LPS
% CD40 and CD86
glucose starved
non-starved
F
5mM glucose
Unt
CP
LPS
LPS+CP
6.27
3.70
58.8
31.6
CD86
HLA-DR
% CD86 and %HLA-DR
G
CD86 (MFI)
HLA-DR (MFI)
scrambled siRNA
PYG siRNA
Medium
LPS
H
Untreated
LPS
Glucose (mM)
Time (hours)
I
Untreated
LPS
Glut1-ib
LPS+Glut1-ib
% CD40 and CD86
ns
6 hour
24 hour

Figure 2. Glycogen Metabolism Supports Survival and Early Maturation of TLR-Activated DCs.

(A and B) 7AAD viability staining of BMDCs stimulated with LPS ± CP for 6 hr (A) and 24 hr (B) at 5 mM glucose.
(C) 7AAD viability staining of moDCs stimulated with LPS ± CP for 24 hr.
(D) BMDCs were stimulated for 6 and 24 hr and analyzed for CD40 and CD86 surface expression.
(E) CD40 and CD86 expression of BMDCs stimulated for 6 hr in free glucose medium with and without glucose starvation.
(F) CD86 and HLA-DR expression of moDCs stimulated with LPS ± CP for 24 hr in 5 mM glucose.
(G) CD86 and HLA-DR surface expression of 24 hr LPS-stimulated moDCs silenced with control (scrambled) or PYG-targeted siRNA.
(H) Glucose measurements from supernatant of BMDCs stimulated with LPS for 3, 6, and 24 hr.
(I) CD40 and CD86 surface expression of BMDCs stimulated ± GLUT1-inhibitor in normal glucose for 6 and 24 hr. (A-F, H-I) n = 3-6, mean ± SD, two-way ANOVA with Tukey's post-test; *p % 0.05, ***p = 0.0006, ****p < 0.0001.
(G) n = 5, paired t test; *p = 0.04, **p = 0.0093.

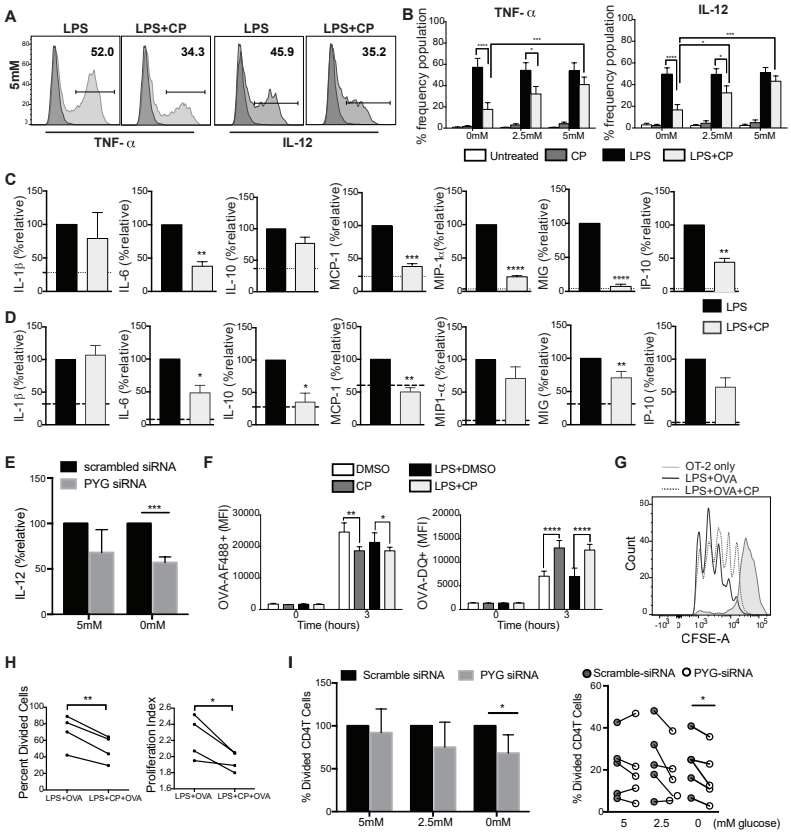

Figure 3. PYG Inhibition Attenuates Immune Effector Functions of DC.

(A) Intracellular staining of TNF-α and IL-12 of BMDCs stimulated with LPS for 4 hr in 5 mM glucose.
(B) Intracellular staining of TNF-α and IL-12 of BMDCs stimulated with LPS for 4 hr in 5, 2.5, and 0 mM glucose.
(C and D) Multiplex panels of cytokine and chemokine measurements from the supernatant of BMDCs (C) and moDCs (D) activated with LPS for 6 hr. Dotted lines represent unstimulated levels.
(E) Relative IL-12 production by moDCs LPS-stimulated for 24 hr transfected with control or PYG-targeted siRNA.
(F) BMDCs treated with LPS ± CP plus OVA-AF488 or OVA-DQ for 3 hr and analyzed by flow cytometry for antigen uptake and processing.
(G) BMDCs were pulsed for 6 hr with indicated treatments and subsequently co-cultured with CFSE-labeled OT-II T cells. CFSE dilution was measured on day 3 post co-culture.
(H) Measurements of proliferation of OT-II T cells (from G) stimulated by BMDCs pre-treated with indicated conditions.
(I) siRNA transfected moDCs were co-cultured with CellTrace Violet-labeled human naive $CD4^+$ T cells for 4 days. Data were normalized to scrambled siRNA. Proliferation was measured after 4 days.
(A-I) n = 3-5, mean ± SD. (B and F) Two-way ANOVA Tukey's post-test. (C–E, H, and I)

Student's t test; *p % 0.05, **p < 0.001, ***p = 0.0004, ****p < 0.0001.

Glycogen-Derived Carbons Fuel Both Glycolytic Reprogramming and Mitochondrial Respiration in Activated DCs

We proposed that glycogen-derived glucose drives early glycolytic flux in TLR-activated DCs prior to GLUT1 upregulation. To test this, we performed a real-time extracellular flux analysis on BMDCs and moDCs. LPS-driven glycolytic burst was significantly attenuated by PYG inhibition in both BMDCs (Figures 4A and S3A) and moDCs (Figure 4B). We further tested whether cell-intrinsic glycogen metabolism also contributes to mitochondrial respiration during early activation. Concomitant with glycolysis reduction, PYG inhibition attenuated the oxygen consumption rate (OCR) in BMDCs regardless of activation (Figure 4C). These data suggest that pre-existing glycogen pools contribute metabolic substrates for mitochondrial respiration. Consistent with this, PYG inhibition accelerates LPS-mediated ATP depletion during early activation in a time-dependent manner (Figure 4D). The synergistic effect of combined CP and ATP-synthase inhibitor oligomycin in reducing ATP production (Figure 4E) indicates that glycogen catabolism contributes to both cytosolic and mitochondrial ATP generation. These findings indicate the intriguing possibility that there may be distinct roles for glucose and glycogen-derived carbon molecules in DC metabolism.

Since PYG inhibition resulted in reduced intracellular ATP levels (Figures 4D and 4E), we assessed the effect of PYG inhibition on the activation of AMPK, a key metabolic sensor of intra-cellular nutrient and ATP levels [28]. PYG inhibition resulted in increased phosphorylation of AMPK (Figure S3B), which is reported to antagonize BMDC activation [10]. This is consistent with reports showing that inhibition of glycolysis induces compensatory activation of AMPK [29, 30]. However, PYG inhibition had no impact on LPS-mediated GLUT1 upregulation (Figure S3C), suggesting that AMPK regulation of glucose transport is not a significant mechanism at play in our model. Nevertheless, LKB1 deficient BMDCs, which are incapable of activating AMPK, show decreased sensitivity to PYG inhibition during maturation at normal glucose concentrations, suggesting that AMPK compensatory activation during PYG inhibition may be involved in regulating maturation in these conditions (Figure S3D).

Previous work has demonstrated that glucose consumed by activated DCs enters the TCA cycle to generate citrate, which is preferentially translocated from the mitochondria into the cytosol via the citrate shuttle to support *de novo* fatty acid synthesis. This process is linked to ER and Golgi membrane expansion, which is hypothesized to enhance the production of effector molecules central to DC activation [8, 11]. To examine the role of glycogenolysis in citrate metabolism explicitly, we performed metabolic tracing experiments in

which BMDCs were differentiated in ^{13}C-labeled glucose to label all intracellular metabolites. Cells were subsequently switched to normal glucose at the time of LPS stimulation in the presence or absence of CP for 1 and 3 hr. As previously published, LPS stimulation induces substantial metabolic flux through glycolysis and TCA citrate production ([31] and data not shown). PYG inhibition significantly reduced ^{13}C-labeled citrate while no statistically significant impact on hexose phosphate, pyruvate, lactate, and post-citrate metabolites fumarate and malate was observed (Figures 4F and S3E). Hexose phosphate refers to any 6-carbon sugar since our metabolite tracing approach could not distinguish individual sugars among this group. These data indicate that intracellular glycogen reserves preferentially support the generation of citrate following LPS stimulation.

Glutamine can also serve as an important carbon source for the TCA cycle. However, the findings that nearly the entire glutamine pool is derived from ^{12}C-labeled sources (Figure S3F) and that CP has very little effect on glutamine levels (Figure S3F) suggest that glutamine metabolism is not directly impacted by PYG inhibition. This is further supported by observations that (1) CP attenuates the maturation of BMDCs stimulated in the presence or absence of glutamine (Figure S3G) and (2) glutaminolysis inhibitor DON has no significant impact on glycolytic burst or OCR (Figure S3H).

To identify the role of glycogen metabolism in regulating extra-cellular glucose flux, the reverse metabolomics experiment was performed in which BMDCs differentiated in normal glucose were switched to ^{13}C-glucose at the time of LPS activation and analyzed at 3 and 6 hr post stimulation (Figure 4G). PYG inhibition minimally affected the ^{13}C-glucose contribution to cytoplasmic hexose phosphate, lactate, and pyruvate, while it severely attenuated both ^{12}C- and ^{13}C-glucose contributions to citrate production (Figure 4G).

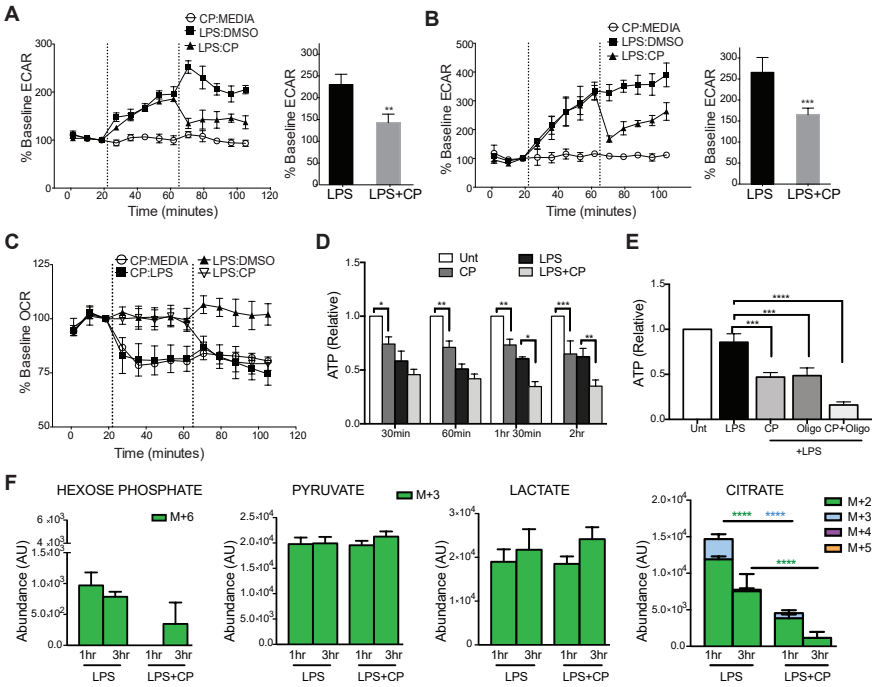

Figure 4. Glycogen-Derived Carbons Fuel Early Glycolytic Reprogramming and Mitochondrial Respiration in Activated DCs.

(A and B) Real-time changes in ECAR of BMDCs (A) and moDCs (B).
(C) Real-time changes in OCR of BMDCs.
For (A)–(C), treatments were introduced at dotted lines (first injection: second injection).
(D and E) ATP levels of BMDCs in 30 min intervals (D) and at 2 hr (E) after stimulation with indicated treatments.
(F) BMDCs cultured and differentiated in $^{13}C_6$-glucose were switched to normal glucose at the time of stimulation with LPS ± CP for 1 and 3 hr, and ^{13}C-labeled metabolites were detected by LC-MS spectrometry.
(G) Inverse metabolomics of (F), where BMDCs were differentiated in normal ^{12}C-glucose and switched to $^{13}C_6$-glucose at the time of stimulation with LPS ± CP for 3 and 6 hr.
Data represent n = 4, mean ± SD; (A and B) paired Student's t test; (D-G) n = 5, two-way ANOVA, Tukey's post-test. *p < 0.05, **p < 0.005, ***p < 0.0005, ****p < 0.0001.
(F and G) Statistical significance of each color * represents color-coded $^{13}C_6$ or black * for ^{12}C groups. White bars indicate l2C-glucose, and all color bars denote $^{13}C_6$-glucose.

The metabolite tracing data are consistent with previously published work [31] in which extracellular glucose contributes heavily to cytoplasmic glycolytic metabolites and citrate production from the TCA cycle (Figures 4F and 4G). However, these data also uncover two previously unappreciated aspects of glucose metabolism in DCs: (1) glycogen-derived carbons from basal glycogen stores (CP-sensitive ^{13}C metabolites in Figure 4F) preferentially support initial glycolytic intermediates and citrate synthesis; (2) a significant amount of

glucose imported from the extracellular environment gets rapidly converted into glycogen (CP-sensitive ^{13}C metabolites in Figure 4G). The finding that extracellular ^{13}C-glucose incorporation into citrate (Figure 4G), succinate, fumarate, and malate (Figure S3I) is sensitive to PYG inhibition suggests that a significant portion of extracellular glucose destined for mitochondrial oxidation is metabolically routed via a glycogen-dependent pathway during DC activation. The routing of glucose carbons via a rapid sequence of glycogen synthesis and glycogenolysis is characteristic of a metabolic pathway described in astrocytes and muscle cells as the ''glycogen shunt'' [32, 33]. Our metabolic profiling studies support a model where glucose processing in TLR-stimulated DCs undergoes three functionally distinct pathways: (1) the catabolism of pre-activation intracellular glycogen stores; (2) the catabolism of imported glucose directly; (3) the incorporation of imported glucose into synthesis and breakdown of glycogen via the glycogen shunt (modeled in Figure S4).

While the glycogen shunt is clearly inefficient from an energetic perspective, others have argued that glycogen breakdown and synthesis may occur in separate spatial pools within brain and muscle cells to fuel rapid bursts of metabolic activity required in these cells that override the total energetic cost of this process [34-36]. DCs may employ a similar strategy of compartmentalized glycogen metabolism in order to fuel early immune activation. However, how this occurs and how it may be regulated in DCs remains an important question. Precedent for distinct and parallel sugar metabolism has been previously reported, whereby granulocyte phagocytic capability is driven by glycogen-derived carbons, while their chemotaxis is fueled by catabolism of free glucose carbons [37]. We propose that the source of carbons in activated DCs, namely whether it is glucose or glycogen derived, may dictate differential functional responses. We speculate that spatial compartmentalization of these processes in the cytoplasm may be an important component of how glycogen metabolism is regulated.

While glycogen metabolism has been previously implicated in myeloid cells of the immune system [21, 37-40], the role of glycogen metabolism in specific immune effector functions of DCs has not been previously defined. We show here a definitive role for glycogen metabolism in regulating immune effector functions of both human and mouse DCs. We further demonstrate that glucose- and glycogen-derived carbons exhibit distinct metabolic fates, a phenomenon that we suspect is not DC specific and likely occurs in other cells that utilize cell-intrinsic glycogen metabolism. Ongoing studies are focused on elaborating the mechanistic details of how glycogen-dependent compartmentalization of metabolic pathways occurs in response to different immune stimuli. With a growing interest in understanding how metabolic regulation controls

the functional effector responses of immune cells, this work delineates an intricate and novel layer of complexity to how metabolic pathways operate at a subcellular level, which may be exploited in cell-based therapeutic applications in the future.

Author contributions

Conceptualization, P.T. and E.A.; Methodology, P.T., A.D., B.E., and E.A.; Formal Analysis, P.T., J.A.R., and A.D.; Investigation, P.T., L.R.P., R.C., B.E., S.B., J.A.R., A.D., and E.A.; Writing – Original Draft, P.T. and E.A.; Writing – Review & Editing, P.T., L.R.P., A.D., B.E., and E.A.; Funding Acquisition, E.A.; Resources, A.D., B.E., and E.A.; Supervision, A.D., B.E., and E.A.

Acknowledgements

The authors would like to acknowledge the UVM core facilities (Flow Cytometry, Animal Resource, Microscopy Imaging, and Advance Genome Technology Cores) for services provided in support of this work. Special acknowledgment to Dr. Ralph Budd, Dr. Paula Deming, and the VCIID COBRE for extensive support. Thank you to Dr. Matt Poynter for OVA-AF488 and OVA-DQ reagents. Funding sources: Boettcher Webb-Waring Biomedical Research - Early Career grant (2017) (A.D.), Veni Fellowship NWO (Grant# 91614087) (B.E.), LUMC fellowship (B.E.), 2016 AAI Careers in Immunology Fellowship (P.T. and E.A.), UVM College of Nursing and Health Sciences Incentive Grant (E.A.), UVM start-up Funds (E.A.), and P30GM118228 (E.A.).

References

1. Banchereau, J. and R.M. Steinman, *Dendritic cells and the control of immunity.* Nature, 1998. **392**(6673): p. 245-52.
2. Lee, H.K. and A. Iwasaki, *Innate control of adaptive immunity: dendritic cells and beyond.* Semin Immunol, 2007. **19**(1): p. 48-55.
3. Lipscomb, M.F. and B.J. Masten, *Dendritic cells: immune regulators in health and disease.* Physiol Rev, 2002. **82**(1): p. 97-130.
4. Akira, S. and K. Takeda, *Toll-like receptor signalling.* Nat Rev Immunol, 2004. **4**(7): p. 499-511.
5. Amati, L., et al., *Toll-like receptor signaling mechanisms involved in dendritic cell activation: potential therapeutic control of T cell polarization.* Curr Pharm Des, 2006. **12**(32): p. 4247-54.
6. Barton, G.M. and R. Medzhitov, *Control of adaptive immune responses by Toll-like receptors.* Curr Opin Immunol, 2002. **14**(3): p. 380-3.
7. Amiel, E., et al., *Inhibition of mechanistic target of rapamycin promotes dendritic cell activation and enhances therapeutic autologous vaccination in mice.* J Immunol, 2012. **189**(5): p. 2151-8.
8. Amiel, E., et al., *Mechanistic target of rapamycin inhibition extends cellular lifespan in dendritic cells by preserving mitochondrial function.* J Immunol, 2014. **193**(6): p. 2821-30.
9. Everts, B., et al., *Commitment to glycolysis sustains survival of NO-producing inflammatory dendritic cells.* Blood, 2012. **120**(7): p. 1422-31.
10. Krawczyk, C.M., et al., *Toll-like receptor-induced changes in glycolytic metabolism regulate dendritic cell activation.* Blood, 2010. **115**(23): p. 4742-9.
11. Rehman, A., et al., *Role of fatty-acid synthesis in dendritic cell generation and function.* J Immunol, 2013. **190**(9): p. 4640-9.
12. Everts, B. and E.J. Pearce, *Metabolic control of dendritic cell activation and function: recent advances and clinical implications.* Front Immunol, 2014. **5**: p. 203.
13. Fox, C.J., P.S. Hammerman, and C.B. Thompson, *Fuel feeds function: energy metabolism and the T-cell response.* Nat Rev Immunol, 2005. **5**(11): p. 844-52.
14. Pearce, E.J. and B. Everts, *Dendritic cell metabolism.* Nat Rev Immunol, 2015. **15**(1): p. 18-29.
15. Pearce, E.L. and E.J. Pearce, *Metabolic pathways in immune cell activation and quiescence.* Immunity, 2013. **38**(4): p. 633-43.
16. Freemerman, A.J., et al., *Metabolic reprogramming of macrophages: glucose transporter 1 (GLUT1)-mediated glucose metabolism drives a proinflammatory phenotype.* J Biol Chem, 2014. **289**(11): p. 7884-96.
17. Macintyre, A.N., et al., *The glucose transporter Glut1 is selectively essential for CD4 T cell activation and effector function.* Cell Metab, 2014. **20**(1): p. 61-72.
18. Adeva-Andany, M.M., et al., *Glycogen metabolism in humans.* BBA Clin, 2016. **5**: p. 85-100.
19. Roach, P.J., et al., *Glycogen and its metabolism: some new developments and old themes.* Biochem J, 2012. **441**(3): p. 763-87.

20. Voet, D., J.G. Voet, and C.W. Pratt, *Fundamentals of biochemistry: life at the molecular level*. 2016: John Wiley & Sons.
21. Maroof, A., et al., *Developing dendritic cells become 'lacy' cells packed with fat and glycogen.* Immunology, 2005. **115**(4): p. 473-83.
22. Afzelius, B.A., *Section staining for electron microscopy using tannic acid as a mordant: a simple method for visualization of glycogen and collagen.* Microsc Res Tech, 1992. **21**(1): p. 65-72.
23. Favaro, E., et al., *Glucose utilization via glycogen phosphorylase sustains proliferation and prevents premature senescence in cancer cells.* Cell Metab, 2012. **16**(6): p. 751-64.
24. O'Neill, L.A., *Glycolytic reprogramming by TLRs in dendritic cells.* Nat Immunol, 2014. **15**(4): p. 314-5.
25. Pearce, E.L., et al., *Enhancing CD8 T-cell memory by modulating fatty acid metabolism.* Nature, 2009. **460**(7251): p. 103-7.
26. Lawless, S.J., et al., *Glucose represses dendritic cell-induced T cell responses.* Nat Commun, 2017. **8**: p. 15620.
27. Wieman, H.L., J.A. Wofford, and J.C. Rathmell, *Cytokine stimulation promotes glucose uptake via phosphatidylinositol-3 kinase/Akt regulation of Glut1 activity and trafficking.* Mol Biol Cell, 2007. **18**(4): p. 1437-46.
28. Hardie, D.G., F.A. Ross, and S.A. Hawley, *AMPK: a nutrient and energy sensor that maintains energy homeostasis.* Nat Rev Mol Cell Biol, 2012. **13**(4): p. 251-62.
29. Wang, Q., et al., *2-Deoxy-D-glucose treatment of endothelial cells induces autophagy by reactive oxygen species-mediated activation of the AMP-activated protein kinase.* PLoS One, 2011. **6**(2): p. e17234.
30. Wu, Y., et al., *Combined inhibition of glycolysis and AMPK induces synergistic breast cancer cell killing.* Breast Cancer Res Treat, 2015. **151**(3): p. 529-39.
31. Everts, B., et al., *TLR-driven early glycolytic reprogramming via the kinases TBK1-IKKvarepsilon supports the anabolic demands of dendritic cell activation.* Nat Immunol, 2014. **15**(4): p. 323-32.
32. Shulman, R.G., F. Hyder, and D.L. Rothman, *Cerebral energetics and the glycogen shunt: neurochemical basis of functional imaging.* Proc Natl Acad Sci U S A, 2001. **98**(11): p. 6417-22.
33. Shulman, R.G. and D.L. Rothman, *The "glycogen shunt" in exercising muscle: A role for glycogen in muscle energetics and fatigue.* Proc Natl Acad Sci U S A, 2001. **98**(2): p. 457-61.
34. Calder, P.C. and R. Geddes, *Heterogeneity of glycogen synthesis upon refeeding following starvation.* Int J Biochem, 1992. **24**(1): p. 71-7.
35. Elsner, P., et al., *Partly ordered synthesis and degradation of glycogen in cultured rat myotubes.* J Biol Chem, 2002. **277**(7): p. 4831-8.
36. Obel, L.F., et al., *Brain glycogen-new perspectives on its metabolic function and regulation at the subcellular level.* Front Neuroenergetics, 2012. **4**: p. 3.
37. Weisdorf, D.J., P.R. Craddock, and H.S. Jacob, *Glycogenolysis versus glucose transport in human granulocytes: differential activation in phagocytosis and chemotaxis.* Blood, 1982. **60**(4): p. 888-93.
38. Scott, R.B., *Glycogen in human peripheral blood leukocytes. I. Characteristics of the synthesis and turnover of glycogen in vitro.* J Clin Invest, 1968. **47**(2): p. 344-52.

39. Yunis, A.A. and G.K. Arimura, *ENZYMES OF GLYCOGEN METABOLISM IN WHITE BLOOD CELLS. I. GLYCOGEN PHOSPHORYLASE IN NORMAL AND LEUKEMIC HUMAN LEUKOCYTES.* Cancer Res, 1964. **24**: p. 489-92.
40. Yunis, A.A. and G.K. Arimura, *Enzymes of glycogen metabolism in white blood cells. II. Activation and inactivation of glycogen phosphorylase of rat chloroma.* Biochim Biophys Acta, 1966. **118**(2): p. 325-34.

Methods

Mouse Models

The University of Vermont's Animal Facility is a barrier facility housing only mice. All animals are housed in autoclaved Lab Products microisolator cages on ventilated racks and handled using aseptic technique in laminar flow work stations and are provided with sterile water and irradiated rodent chow (Lab Diets Isopro RMH 3000). Mice are maintained in a pathogen free environment at a constant temperature and humidity, with 12-hour light and 12-hour dark cycle. Personnel wear shoe covers, isolation gowns, masks, bouffant and exam gloves. In addition, animal husbandry personnel wear dedicated scrubs and footwear. Health monitoring of colony and sentinel animals is performed quarterly. The University's program of animal care has been fully-accredited by AAALAC, International for over 25 years. OT-II (B6.Cg-Tg (TcraTcrb)425Cbn/J and C57/Bl6J mice mice were purchased from Jackson Laboratory and were maintained at the University of Vermont animals care facility under protocols approved by Institutional Animal Care and Use Committee. For most experiments, adult mice (2-6 months of age) were used. Mouse experiments include data from both male and female mice, however the specific sex distribution for each individual experiment was not explicitly tracked. $Itgax^{cre}$ $LKB1^{fl/fl}$ mice PubMed: 21124450 were housed and bred at the LUMC, Leiden, Netherlands, under SPF conditions. All animal experiments were performed in accordance with local government regulations, and the EU Directive 2010/63EU and Recommendation 2007/526/EC regarding the protection of animals used for experimental and other scientific purposes and approved by the CCD, animal license number AVD116002015253.

Mouse DC Culture and Activation

Bone marrow-derived DCs (BMDCs) were generated as follows: BM cells were flushed from femurs of 9-18-week-old mice and the cells were differentiated in GM-CSF (20 ng/mL; Peprotech) in complete DC medium (CDCM), comprised of RPMI1640, 10% FCS, 2mM L-glutamine, 1 IU/mL Pen-Strep, 1 mM beta-mercaptoethanol, for 7 days, with a medium change every 2 days. On day 7, DCs were washed in CDCM and cultured at 2x10^5 cells per 200 mL of media alone, STF31 (12.5 μM), CP91149 (75-100 μM), DAB (1 mM), LPS (100 ng/mL), LPS plus STF31 or CP91149, or DAB, or OVA (from whole egg white) at indicated time points. Where appropriate, DCs were stimulated in CDCM containing 0 mM, 1.25 mM, 2.5 mM, or 5 mM glucose.

Glucose Starvation Experiment

BMDCs were starved for glucose overnight, with a non-starved group as a control. On the next day, DCs from both groups were washed with sugar free

RPMI and stimulated with LPS in glucose free medium ± CP for 6 hours. CD40 and CD86 expression was analyzed by Flow cytometry.

Human DC Culture and Activation

Human monocyte-derived DCs (moDCs) were differentiated from peripheral blood monocytes as follows: Blood filters from de-identified blood donors were provided by CVPH Medical Center Blood Bank in Plattsburgh, NY. Filters were reverse-flushed in sterile PBS, and PBMCs were prepared by Ficoll-Paque (density gradient of 1.0772) centrifugal separation using LSM media (MP biochemical; Fisher). Resulting monocytes were enriched using CD14 positive selection beads per manufacturer instructions (Miltenyi Bioscience) and cultured in complete DC medium (CDCM) supplemented with human recombinant GM-CSF (20 ng/mL) plus human recombinant IL-4 (20 ng/mL) (Peprotech) for 7 days. On day 7, moDC were harvested, stimulated as indicated, and analyzed by FACS for maturation and by multiplex panels (Life Technologies) for cytokine production.

Quantitative Real-time PCR of *pygl, pygm, gys1,* and *gys2* Expression

RNA was isolated with an RNAeasy Kit (QIAGEN) and cDNA was synthesized with an iScript cDNA Synthesis Kit (Biorad). *pygl*, *pygm*, *gys1*, *gys2*, and *slc2a1* Taqman primer probes (Applied Bioscience system) and AB7500 sequence detection system or QuantStudio 3.0 were used for relative mRNA expression. mRNA relative quantitative values were calculated based on 2(-ΔΔCT) and normalized to untreated samples.

Glycogen Phosphorylase Knockdown by siRNA Transfection of moDC

For knockdown of glycogen phosphorylase isoforms, moDCs were generated as mentioned above. At day 4 of the culture, the cells were harvested, washed with PBS, brought to a concentration of 1x10^6 cells / 100 mL resuspension buffer, and finally, transfected by electroporation with either 10 nM anti-PGYL siRNA in combination with 10 nM anti-PYGB siRNA or 20 nM scrambled siRNA (Dhar- macon). Electroporation was performed using a Neon Transfection System (Invivogen) with the following settings: 1600 V, 20 ms and one pulse. Immediately after electroporation, 1x10^6 cells were taken up in 5 mL 10% HI-FCS basal media, containing no antibiotics, and plated at 200 cells / mL. The next morning, the media was re-supplemented with penicillin, streptomycin, rGM-CSF and rIL-4. At day 6, the cells were harvested, stimulated as indicated, and analyzed by FACS for maturation and by ELISA for cytokine production. Silencing efficiency was determined by qPCR on 6 day-old cells. The transfection efficiency was routinely greater than 80%.

Antigen Uptake, Processing, and In-Vitro T Cell Responses

BMDCs were stimulated ± LPS with OVA-AF488 (5 mg/mL) and OVA-DQ (5 mg/mL) for antigen uptake and processing, respectively. For *in vitro* T cell responses, T cells were generated using mouse CD4 positive selection beads from spleens of 6-10-week-old transgenic OT-II mice and age-matched wild-type B6 mice. BMDCs were pulsed with whole ovalbumin protein (OVA), extracted from egg white, and LPS in the presence or absence of CP for 6 hours, washed 3 times, and co-cultured with CFSE-labeled OT-II T cells at a 1:5 ratio for 72 hours. T cell proliferation (CFSE dilution) was analyzed by flow cytometry.

For alloreaction studies of siRNA transfected moDC, the cells were washed 2 times, and co-cultured with CellTrace Violet-labeled human naive $CD4^+$ T cells, which were isolated using a naive pan T cell isolation kit (Miltenyi) followed by negative selection using CD8 MicroBeads (Miltenyi), at a 1:4 ratio for 4 days. T cell proliferation was analyzed by flow cytometry.

Metabolism Assays

Extracellular glucose and intracellular glycogen levels were measured with a Glucose assay kit (Eton Biosciences) and a Glycogen assay kit (Biovision), respectively. For Biolog assays, (Metabolic phenotypic screening assays), IFM-1 reagent, Biolog MA redox dye, and Biolog plates were purchased from Biolog Inc. Fully differentiated BMDC were plated overnight at 50,000 cells per well in specified nutrient sources in basal MC-0 medium (IFM1 media with 5% FCS, 0.3 mM L-glutamine, 100 I/U Pen Strep). 20 mL of Biolog MA dye was added to each well the next morning. The assays were measured at 592 nm absorbance as indicated. Data were normalized to the readings at time 0. Extracellular acidification rate (ECAR) and oxygen consumption rate (OCR) were measured with Metabolic Flux Analyzer (Seahorse Bioscience, North Billerica, MA 24XP and/or 96XP). ATP concentrations were measured with an ATP Determination Kit (Invitrogen) according to the manufacturer's instructions.

BMDC Cultures and Activation for Metabolomics

For metabolomics tracing in Figure 4F, BMDCs were differentiated in $^{13}C_6$-glucose containing CDCM. On day 7, the cells were switched to $^{12}C_6$-glucose medium, with LPS and LPS+CP added at the time of media switch and stimulated for 1 and 3 hours. At each time point, cells were harvested, counted, pelleted, and frozen for the UHPLC-MLS metabolomics processing below. For inverse metabolomics in Figure 4G, BMDCs normally differentiated in regular CDCM were switched to $^{13}C_6$-glucose medium at the time of stimulation, with and without CP for 3 and 6 hours. Cells were harvested and processed as above. Supernatant from the 6 hour stimulation groups was collected for Multiplex Cytokine analysis.

UHPLC-MS Metabolomics

Frozen cell pellets were extracted at 2e6 cells/mL in ice cold lysis/extraction buffer (methanol:acetonitrile:water 5:3:2). Samples were agitated at 4°C for 30 min followed by centrifugation at 10,000 g for 10 min at 4°C. Protein and lipid pellets were discarded, and supernatants were stored at -80°C prior to metabolomic analysis. Ten mL of extracts were injected into an UHPLC system (Vanquish, Thermo, San Jose, CA, USA) and run on a Kinetex C18 column (150 x 2.1 mm, 1.7 µm – Phenomenex, Torrance, CA, USA) at 250 ml/min (phase A: Optima H_2O, 0.1% formic acid; phase B: acetonitrile, 0.1% formic acid). The autosampler was held at 7°C and the column compartment at 25°C. The UHPLC system was coupled online with a Q Exactive mass spectrometer (Thermo, Bremen, Germany), scanning in Full MS mode (2 mscans) at a 70,000 resolution in the 60-900 m/z range in negative and then positive ion mode (separate runs). Eluate was subjected to electrospray ionization (ESI) with 4 kV spray voltage, 15 sheath gas and 5 auxiliary gas. Metabolite assignments and isotopologue distributions were determined using the software Maven (Princeton, NJ, USA), upon conversion of .raw files into .mzXML format through MassMatrix (Cleveland, OH, USA). Chromatographic and MS technical stability were assessed by determining CVs for heavy and light isotopologues in a technical mixture of extract run every 10 injections. Relative quantitation was performed by exporting the values for integrated peak areas of light metabolites and their isotopologues into Excel (Microsoft, Redmond, CA, USA) for statistical analysis including t test and ANOVA (significance threshold for p values < 0.05).

Electron Microscopy

Samples were fixed in Karnovsky's Fixative for 1hr at 4°C, washed in 0.1 M Cacodylate Buffer, and post-fixed in 1% OsO4 for 1hr at 4°C followed by an extensive rinse with Cacodylate buffer. Samples were then dehydrated in a graded series of ethanol, and embedded in Spurr. Sections were cut with a Reichert Ultracut Microtome and stained with toluidine blue. For contrast, 1% tannic acid was added to the cut sections of the grids for 10 min, followed by 6 min of uranyl acetate and 4 min of lead citrate. Cells were examined with a JEM1400 transmission electron microscope (JEOL USA).

Immunoblot Analysis

Cell lysates were prepared using 2X NP-40 lysis buffer. 20 mg protein was loaded into each well of a 12.5% polyacrylamide gel, transferred onto activated nitrocellulose membrane (BioRad). Electrophoretic transfer was performed using Trans-Blot Turbo RTA mini Nitrocellulose transfer kit. Membranes were blocked in 2% milk in 1xTBST at RT for 1hr, and incubated in indicated antibody at 4°C overnight. Blots were washed 3x in 1xTBST at RT, probed with secondary antibodies at RT for 45-60 min, and washed 3-4x with 1xTBST. Proteins

were visualized by SuperSignal West Pico Chemiluminescent substrate and exposed with GeneXpert System imager. Trans-Blot Turbo Transfer system and secondary antibodies for western blots were generously provided by Dr. Paula Deming, Medical Laboratory and Radiation Science Department, UVM.

Flow Cytometry and Cytokine Measurements

The following fluorescently labeled antibodies were used for flow cytometry: anti-CD11c (N418), anti-CD40 (3/23), anti-CD86 (GL1), IA-b (AF6-120.1), anti-CD1a (HI149), anti-CD40 (5C3), anti-CD86 (IT2.2), anti-TNF-α (MP6-XT22), anti-IL-12p40 (C15.6). Stimulated cells as indicated were harvested and washed in 1% FACS buffer (PBS plus 1% FBS), stained with specific antibodies, and incubated on ice for 30 min. All samples were acquired using a LSRII flow cytometer (BD Biosciences). For intracellular cytokine expression, cells were activated with indicated treatment groups for a total of 4 hours with an addition of Golgi plug (1:1000) (Biolegend) after the first hour of stimulation. For intracellular staining of TNF-α and IL-12 (Biolegend), cells were fixed in 4% paraformaldehyde, permeabilized in 0.2% saponin, and stained with antibodies in FACS buffer (1% FBS in PBS). Samples were analyzed on a BD LSRII flow cytometer. For cytokine levels of BMDCs and moDCs, supernatants were collected as indicated time points and measured with Mouse Cytokine Magentic 20-Plex and Human Cytokine Magnetic 30-Plex panels (Life Technologies) per manufacture instructions using Bio-Plex array suspension system.

Quantification and statistical analysis

Throughout the manuscript, ''n'' refers to independent cell cultures from individual mice or human samples. All the experiments reported in Figure 1 were repeated n = 3-6 mice per condition, with the following detailed n values: Figures 1A–1E and 1I, n = 3; Figures 1F and 1G, n = 6; Figure 1H, n = 4; and Figure 1J, n = 4. The survival and maturation experiments in Figures 2A–2F and S1 were repeated with n = 6. Intracellular cytokine experiments in Figures 3 and S2 were repeated with n = 4. Multiplex analyses in Figures 3 and S2 were repeated with n = 6. All metabolomics experiments in Figures 4 and S3 were repeated with n = 4, and the seahorse experiments in Figures 1, 4, and S3 were repeated with n = 3-5. All the siRNA experiments in Figure 2G, 3I, S1C, and S1D were repeated with n = 5. Data were analyzed with GraphPad Prism software (version 6.0). Samples were analyzed using Student's t test, One-way, and Two-way ANOVA where appropriate. ANOVA tests were post-calculated by Tukey's multiple comparison test or Sidak test. Results are means +/-SD as indicated, and statistical values are represented significant when p values were equal or below 0.05.

Supplementary figures

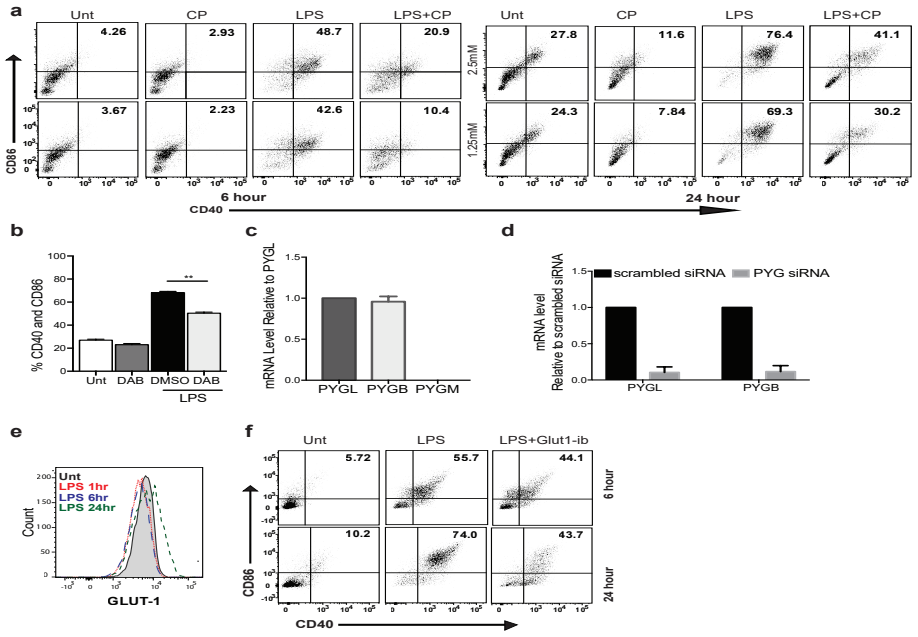

Figure S1. (related to Figure 1 and Figure 2).

(a) BMDCs stimulated with LPS+/-CP for 6 and 24 hours in indicated glucose concentrations were analyzed for CD40 and CD86 surface expression.
(b) CD40 and CD86 expression of BMDCs stimulated with LPS+/-DAB for 6 hours in normal glucose concentration.
(c) mRNA expression of 3 PYG isoforms in moDCs; data normalized to PYGL; n=6.
(d) Relative mRNA level for confirmation of knockdown of pygl and pygb by si-RNA transfection of moDCs.
(e) Intracellular stain of Glut-1 expression in BMDCs stimulated for 1, 6, and 24 hrs.
(f) CD40 and CD86 surface expression of BMDCs stimulated with LPSGlut1-ib for 6 and 24 hours in normal glucose concentration.
(a, e-f) representative of more than 3 experiments. (b) n=4, mean+/-SD, One-way ANOVA with Sidak Post-test,**P=0.0038.

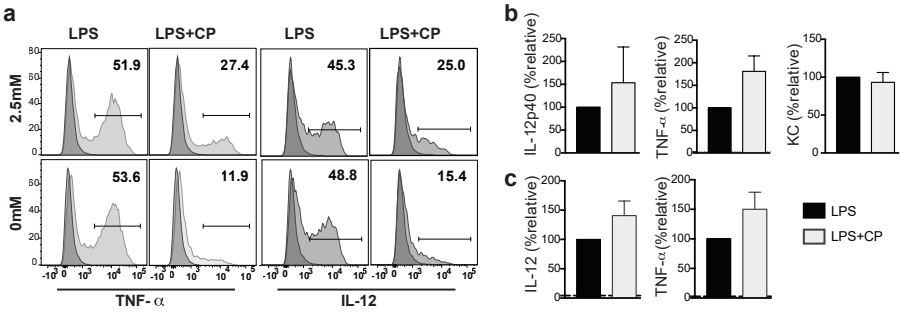

Figure S2. (related to Figure 3).

(a) Intracellular staining of TNF-α and IL-12 of BMDCs stimulated with LPS+/-CP for 4 hours in 2.5 and 0 mM glucose. Data are from one experiment representative of four. (b-c) Multiplex panel of cytokine and chemokine measurements from the supernatant of (b) BMDCs and (c) moDCs activated with LPS+/-CP for 6 hours. Dotted lines represent unstimulated levels. n=4, mean+/-SD, student's t-test.

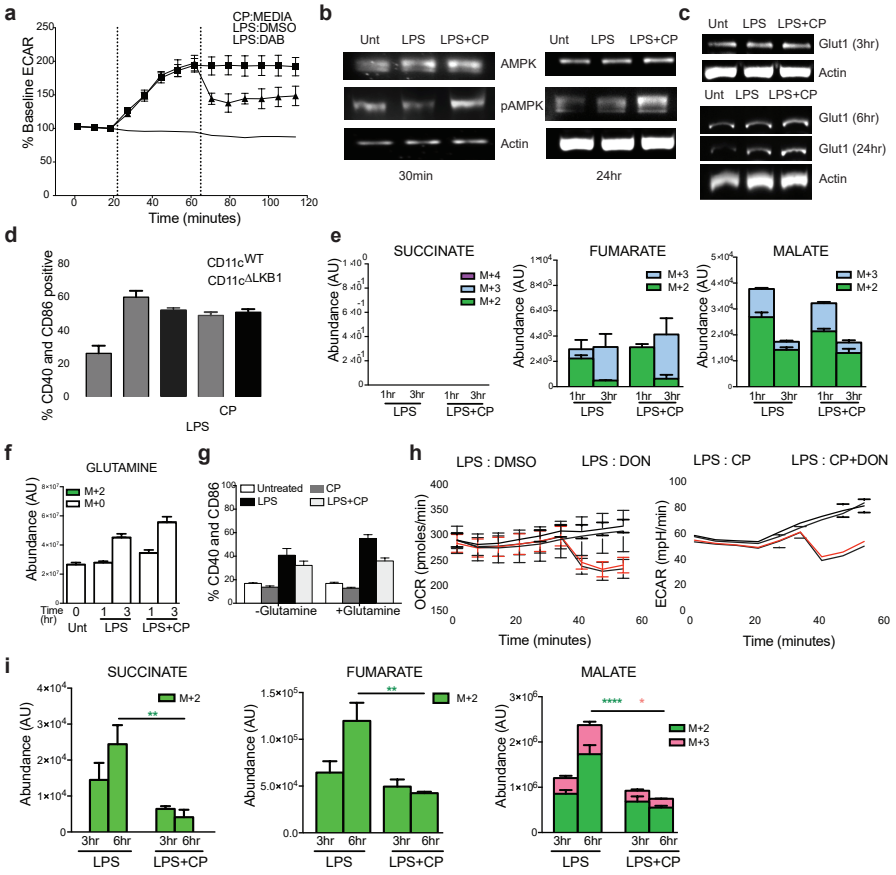

Figure S3. (related to Figure 4).

(a) Real-time changes in ECAR of BMDCs using an alternate PYGL inhibitor, DAB; treatments introduced at dotted lines (1st injection: 2nd injection). Representative of 3 experiments.
(b) Protein expression of AMPK and pAMPK in BMDCs stimulated with LPS+/-CP for 30 minutes and 24 hrs in normal glucose.
(c) Protein expression of Glut-1 in BMDCs stimulated with LPS+/-CP for 3, 6, and 24 hours in normal glucose.
(d) Surface expression of CD40 and CD86 of BMDCs from WT or LKB1-/- mice stimulated with LPS+/- CP for 6 hrs. Data represents replicates n=3. mean+/-SD.
(e,f) BMDCs differentiated in $^{13}C_6$ -glucose were switched to normal glucose at the time of stimulation with LPS+/-CP for 1 and 3 hrs and detected by LC-MS spectrometry. Color bars denote heavy ($^{13}C_6$glucose) whereas white bars represent light ^{12}C glucose.
(e)$^{13}C_6$ glucose not detected in succinate after stimulation.
(g) CD40 and CD86 expression was analyzed in BMDCs stimulated for 6 hours with LPS+/-CP in the presence or absence of glutamine in the medium. n=6
(h) Real-time OCR and ECAR with CP, glutaminolysis inhibitor (DON), or combination; treatment injected at dotted lines (1st injection: 2nd injection).
(i) Inverse metabolite tracing of b and c, where BMDCs differentiated in normal light

glucose were switched to $^{13}C_6$-glucose medium at the time of stimulation with LPS+/-CP for 3 and 6 hrs and selected TCA intermediates were shown. Data represents n=4, mean+/-SD, Two-way ANOVA with Tukey-Post-test. *P=0.019, **P<0.0039, and ****P<0.0001.

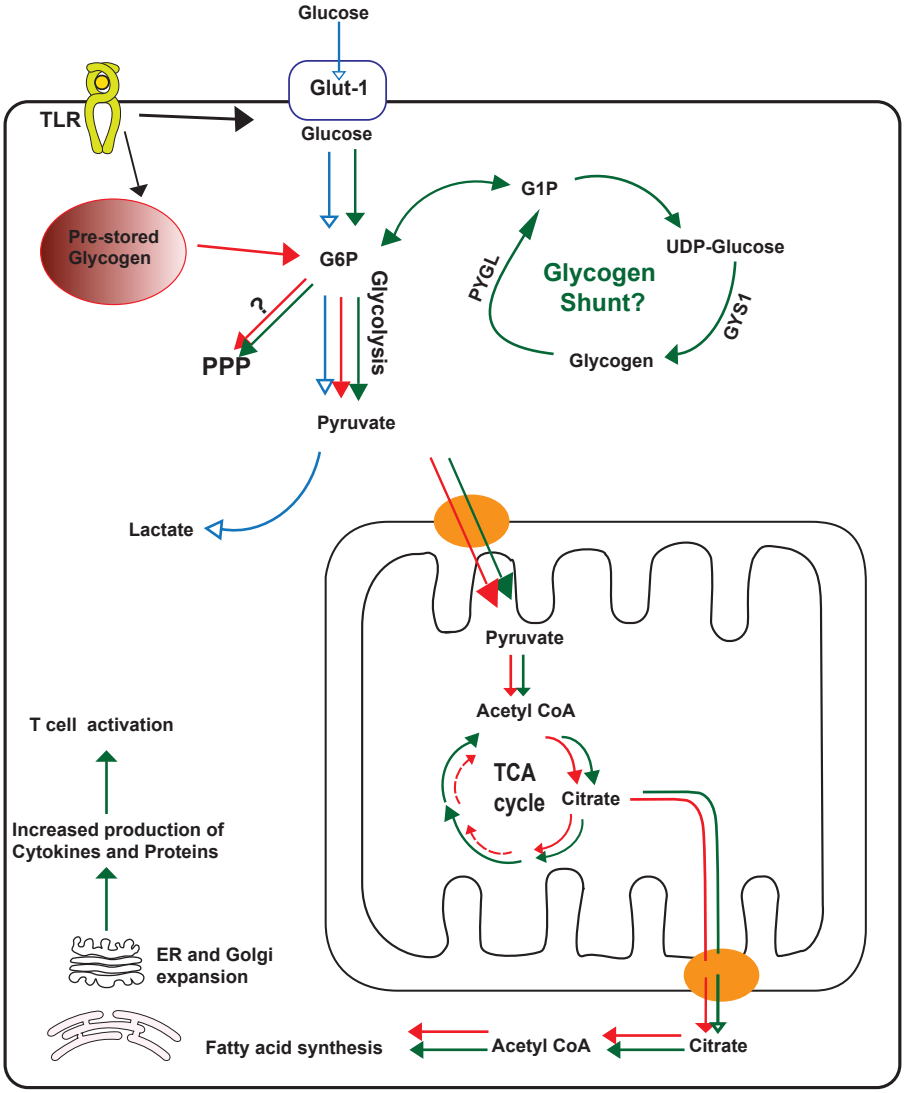

Figure S4. (related to Figure 4).

Proposed Model: Pathway 1 (red) represents the catabolism of basal glycogen stores primarily driving citrate generation. Pathway 2 (blue) represent the catabolism of free glucose which primarily supports the formation of intracellular lactate. Pathway 3 (green) represents glycogen shunt activity, which primarily supports citrate production and a full TCA cycle. PPP=Pentose phosphate pathway